A new probe of ULVZ *S*-wave velocity structure: Array stacking of *ScS* waveforms

Megan Avants,[1] Thorne Lay,[1] and Edward J. Garnero[2]

Received 18 October 2005; revised 2 February 2006; accepted 10 March 2006; published 13 April 2006.

[1] S-wave velocity reductions in thin layers above the core-mantle boundary (CMB) are resolved by modeling precursors to the tangential-components of core-reflected ScS phases. Unlike most phases used to study ultra-low velocity zone (ULVZ) structure, ScS provides direct sensitivity to shear velocity structure, V_S. Recordings of deep earthquakes in the Tonga-Fiji and South American subduction zones at broadband seismic networks in western North America are used to map small-scale ULVZ variability. A two-layer low-V_S structure exists under the central Pacific: an abrupt 0.8–2.0% decrease 60–86 km above the CMB is underlain by a 24–30 km thick ULVZ layer having reductions of 3.3–7.4% (with respect to PREM). No corresponding velocity reductions are found under the Cocos plate. The structure above the ULVZ may be associated with reverse transformation of post-perovskite to perovskite in a steep thermal gradient in a boundary layer above the CMB. **Citation:** Avants, M., T. Lay, and E. J. Garnero (2006), A new probe of ULVZ *S*-wave velocity structure: Array stacking of *ScS* waveforms, *Geophys. Res. Lett.*, *33*, L07314, doi:10.1029/2005GL024989.

1. Introduction

[2] The ultra-low velocity zone (ULVZ) is a thin layer, or discrete mounds, of very low seismic velocity rock located just above the CMB. The ULVZ is intermittently observed, and ranges from 5–40 km in thickness, with *P*-wave velocity (V_P) reductions of 5–10% and estimated *S*-wave velocity (V_S) reductions of 10–30% [e.g., *Garnero et al.*, 1998]. The ULVZ is typically attributed to partial melting, based on the large velocity reductions and observation of a 3:1 ratio in V_S to V_P reductions [*Williams and Garnero*, 1996]. Past studies of the ULVZ have used a variety of seismic phases: SP_dKS [e.g., *Garnero et al.*, 1998]; precursors to *PcP* or *ScP* [e.g., *Rost and Revenaugh*, 2003]; *PKP* scattering [e.g., *Vidale and Hedlin*, 1998], and precursors to *SKS* [*Stutzmann et al.*, 2000]. These phases all provide coupled sensitivity to V_p, V_S and density. Given the importance of the relative behavior of V_S to V_P for inferring the nature of the ULVZ, a method for directly constraining V_S structure is desired.

[3] We study Tonga-Fiji and South American deep earthquakes recorded at western U.S. broadband TRINET and BDSN stations. Stacking enhances any precursors to transverse component *ScS* arrivals arising from abrupt velocity reductions above the CMB. The waveforms are totally insensitive to V_P, and thus provide direct information about V_S and density contrasts.

2. Data and Methods

[4] We analyze 442 horizontal-component *SH* seismograms from 37 intermediate and deep focus Tonga-Fiji events, and 201 *SH* traces from 15 South American events with paths sampling D″ beneath the central Pacific and Cocos Plate, respectively (Figure 1). Magnitudes (m_b) are 5.7 and larger, and epicentral distances range from 74–83°. All data are deconvolved by instrument responses to obtain ground displacement, corrected for lithospheric anisotropy beneath the stations, and rotated to the great circle reference frame. The *SH* displacement records are high-pass filtered using a two-pass Butterworth filter with the low frequency cutoff ranging from 0.005 Hz to 0.02 Hz, depending on signal quality. Traces for a given event are then normalized relative to the *ScS* peak amplitude and linearly stacked to produce an average source wavelet. The source wavelet is tapered and windowed to extract a positive wavelet with no precursor and limited coda, and then deconvolved from all traces for that event using a water-level deconvolution (with uniform water level of 0.0001 for all but 3 larger events with values up to 0.01). A low-pass filter with corner frequency of 0.3 Hz is then applied to each trace, yielding filtered spike trains with consistent signal shape and bandwidth between all records. *ScS* is used to estimate the source wavelet because more stable deconvolutions are obtained than when using the broader source wavelets found by stacking *S*.

[5] Figure 2a shows a sample displacement trace before source deconvolution. Figure 2b shows the *ScS* source wavelet obtained for this event by stacking 48 records, which is deconvolved from the trace in Figure 2a to yield that shown in Figure 2c. In Figure 2c, *S* and *ScS* are simplified spikes, and the *ScS* arrival is preceded by precursory energy that is not present for *S*. We focus our attention on the 10 s window just before *ScS*, well separated from *S* and its strong coda. Deconvolution and filtering produce sidelobes and some ringing of the waveforms, so one must both stack multiple observations to suppress noise and model the stacks by synthetics with similar processing artifacts to provide a reliable interpretation of any ScS precursors. *Avants et al.* [2006] show many additional individual deconvolved waveforms for our data set.

[6] Figure 3 shows the results of stacking all stable deconvolutions for each of 7 events, focusing on the 10 s interval before *ScS*. Source deconvolution results in stable, consistent *ScS* waveforms between events, and the data

[1]Earth Sciences Department, University of California, Santa Cruz, California, USA.
[2]Department of Geological Sciences, Arizona State University, Tempe, Arizona, USA.

0094-8276/06/2005GL024989$05.00

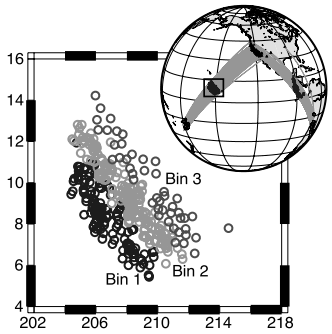

Figure 1. Map: The central Pacific study region showing *ScS* CMB reflection points with the symbols indicating which data go into the 3 data bins corresponding to Figure 5. Inset: Tonga-Fiji and South America earthquakes (solid circles), *ScS* raypaths and CMB reflection points (circles), and broadband BDSN and TERRAscope/TRINET station locations (triangles).

were aligned on the *ScS* peaks before stacking. The direct *S* energy arrives in the interval from 15 to 40 s ahead of *ScS* and does not stack coherently; thus it is unlikely that any late receiver coda will align to give precursory energy to *ScS*. The event stacks are ordered from top to bottom with increasing distance from California. The two most distant events show strong positive energy arriving more than 10 s ahead of *ScS*; this is energy reflected from the top of D″. Two negative peaks can be identified in the 10 s interval before *ScS* for all but the two most distant events. Earlier energy and coda after *ScS* are not coherent between event stacks. The coherent *ScS* precursors can be further enhanced by stacking all combinations of stations and sources.

[7] We double-array stack [*Reasoner and Revenaugh*, 1999] our *ScS* data to improve the signal-to-noise ratio for the *ScS* precursors. This procedure uses a 1-D reference velocity model (in this case PREM [*Dziewonski and Anderson*, 1981]) and calculates the differential time shifts between a reference phase (here, *ScS*) and top-side pre-critical reflections from a suite of specified target depths. We align data on the *ScS* peaks, normalizing the *ScS* amplitudes to unity. The V_S value of the reference velocity model at the base of the mantle is artificially extrapolated downward into the core to enable stacking of energy arriving after *ScS*. The double-array stack for 442 recordings of 37 Tonga-Fiji events is shown in Figure 4a. Direct *S* turns above the depth range shown and the S arrivals are masked to suppress any energy from *S* and its early coda. The deconvolution bandwidth and background velocity model (PREM) used in the stacking algorithm determine the depth extent of the feature associated with *ScS*, and the low-frequency filtering causes a slight negative baseline shift of the stack. A negative peak (A) is imaged 30–40 km above the CMB, and there is a secondary negative feature at an apparent depth near 100 km (B) above the CMB. A broad positive feature is imaged at depths from 200–300 km above the CMB; this is SdS energy reflected from the top of D″ in this region, [see *Avants et al.*, 2006]. The double-array stack of synthetics for PREM computed by the reflectivity

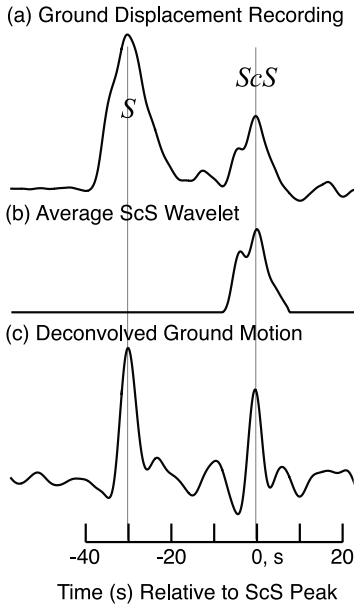

Figure 2. (a) Representative transverse-component displacement seismogram from the Tonga-Fiji data event on April 28, 2001, recorded at station KCC. *S* and *ScS* arrivals are labeled. (b) Average source wavelet for this event, obtained by stacking *ScS* observations. (c) Deconvolution of the trace in Figure 2a by the wavelet in Figure 2b yields this signal after band-pass filtering (corner frequencies 0.005 Hz and 0.3 Hz).

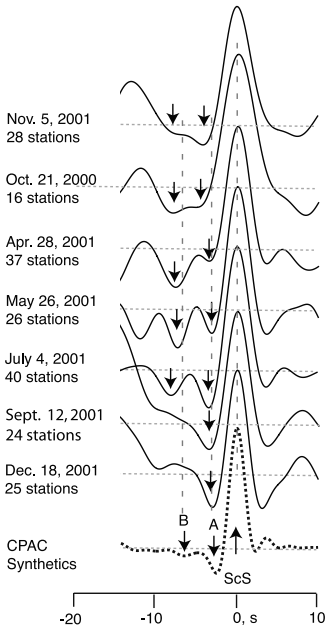

Figure 3. Stacks of the indicated number of deconvolved seismograms for each event, aligned on *ScS,* ordered by increasing event distance from California from top to bottom. Two stable negative amplitude peaks in the 10 s window before *ScS* are observed in the five closer events, with only one precursor being observed for the two more distant events. A stack of synthetics for model CPAC (Figure 4c), which fits the composite stack of all waveforms in this region (Figure 4b) is shown at the bottom as a reference. Direct S energy arrives 10–25 s before the windows shown.

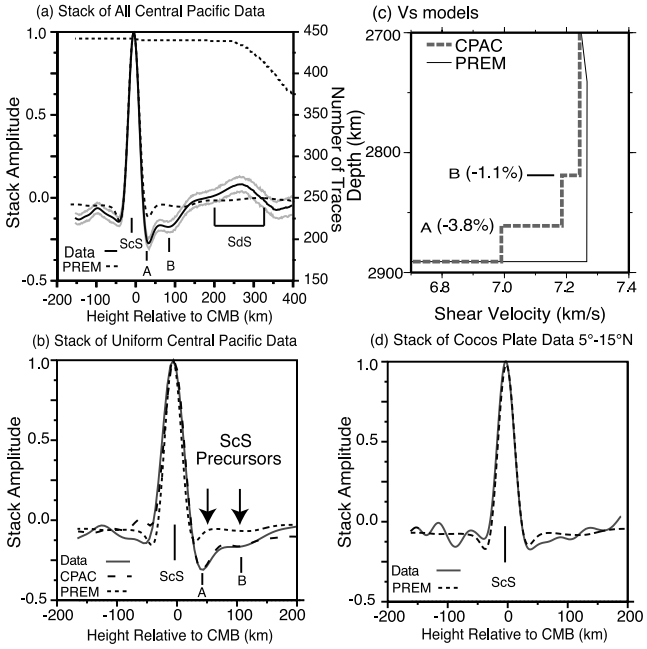

Figure 4. (a) Double-array stack for 442 deconvolved waveforms sampling the central Pacific region (line), with boot-strap variance estimates on the stack (light gray bounds). The data are aligned on *ScS*, and form a strong peak at a reference depth corresponding to the CMB. A stack of synthetics for PREM (dashed line) highlights the two negative *ScS* precursor features (A) and (B) and the positive energy from reflections at the top of D″ (*SdS*). The number of traces contributing to the stack at each depth is shown by the dotted line and the scale on the right. (b) Double-array stack of a subset of 339 traces from the central Pacific study region for events with uniform bandwidth deconvolutions (line) showing two small precursors to *ScS*, with superimposed stacks of synthetics for PREM (dotted line) and model CPAC (dashed line). (c) *S*-wave velocity profile for the average central Pacific model CPAC (dashed line) and PREM (dark gray line). (d) Double-array stack of 201 traces sampling the Cocos Plate study region from 5–15°N (line) and stack of synthetics for PREM (dotted line).

method and processed in the same way as the data, indicates that these arrivals are not expected for a smooth velocity model.

[8] Figure 4b shows the double-array stack for 339 waveforms from 34 Tonga-Fiji events with uniform deconvolution bandwidth. The A and B precursors clearly stand out relative to the baseline defined by the PREM synthetics, and are well matched by stacks of synthetics for model CPAC (Figure 4c), which has a 3.8% V_S reduction (relative to PREM) 30 km above the CMB (discontinuity A), and a 1.1% V_S reduction 72 km above the CMB (discontinuity B). Similar processing of the data sampling the Cocos Plate region yields the double-array stack in Figure 4d, which has no significant negative amplitude features above the CMB, and is closely matched by a double-array stack of synthetics for PREM.

[9] Previous work has demonstrated that there is a southwest to northeast gradient in shear-wave velocity and shear-wave splitting [*Russell et al.*, 1999] and in the depth of the D″ discontinuity [*Avants et al.*, 2006] in our central Pacific study region. Thus, we subdivide our uniform bandwidth data into 3 slightly overlapping bins that follow this trend (Figure 1), and stack the data having *ScS* CMB reflection points in each bin to examine lateral variation in the timing and strength of the *ScS* precursors.

[10] We construct localized two-layer Vs models for each bin. We adjust the thickness and V_S reduction of the deepest layer, which we call the ULVZ (giving rise to the negative stack amplitude A in Figure 4b), as well as thickness and V_S reduction of a shallower layer (giving negative stack amplitude B in Figure 4b). The density structure in these models is kept the same as PREM as we cannot resolve the trade-off between shear velocity increase and density decrease. The magnitudes of the V_S reductions in the ULVZ layer are consequently a maximum, assuming a density increase there, while slight underestimation of the V_S reduction of the B discontinuity could occur if the density decreases at that boundary, as discussed below.

[11] Our synthetic stacks predict underside multiples within the low velocity layers, which image below the CMB in the double array stack (arriving after *ScS* in the waveforms). These features correlate loosely with some energy in the data stacks (small peaks at approximately 130 and 70 km below the CMB in the data stack in Figure 4b), but the timing and amplitude of the features are not well matched. Varying the density, V_S, and thickness of the low velocity layers was explored, but it proves difficult to match the subtle data features arriving after *ScS*. We observe strong variations in the deconvolved seismograms after *ScS* (Figure 3) which may be due to receiver structure, underestimation of the tail of the source wavelet, underside reflections from near-source layering, or signal-generated noise, all of which should be manifested after *ScS*, but not important before *ScS*. Consequently, we emphasize matching the timing and amplitude of *ScS* precursors in developing our preferred V_S models.

3. Results

[12] The results of stacking and modeling the three subregions are shown in Figure 5. Bin 1 (see map, Figure 1), has the ULVZ (precursor A) modeled with a 24 km thickness and a 3.3% V_S decrease, while precursor B, is modeled by a 0.8% V_S decrease 61 km above the CMB (Figure 5a). This bin corresponds to data furthest from the stations, and as apparent in Figure 3, precursor B is weak at larger distances. The fit to the data stack is not good at depths more than 150 km above the CMB, possibly because there is a positive gradient or fine scale shallower structure that we have not modeled. The data stack for Bin 2 was fit by a model with a 29 km thick ULVZ with a 7.4% V_S decrease and a B discontinuity with a V_S reduction of 2.0% 60 km above the CMB (Figure 5b). Bin 3 was modeled with a 30 km thick ULVZ (precursor A) with a 6.3% V_S decrease, and a B discontinuity 86 km above the CMB with a 1.9% V_S reduction (Figure 5c).

[13] Extensive suites of models were run to gain insight into the resolution of the modeling; there are trade-offs with the absolute velocity levels, but acceptable matches to the data for a given baseline structure are found for velocity decreases within about 0.2% and depths within ±3 km of the

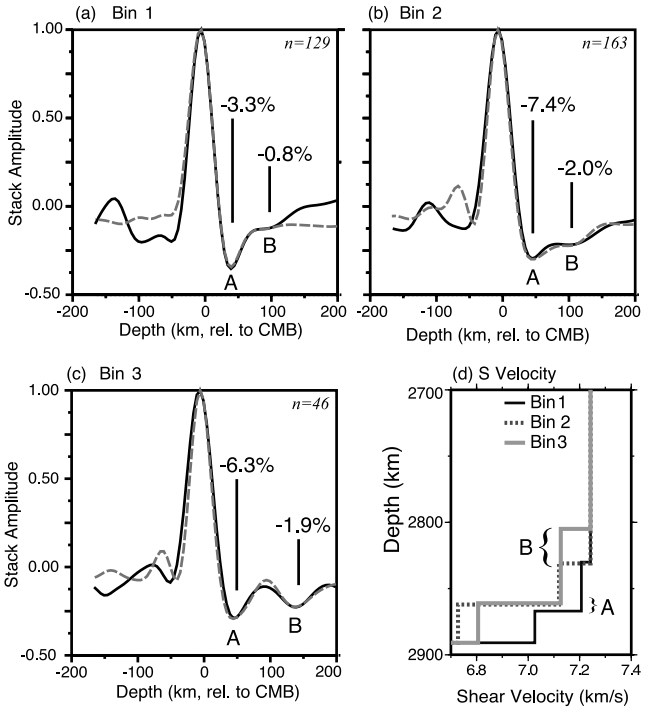

Figure 5. Double-array stacks of data (lines) and synthetics (dashed lines) for (a) Bin 1, (b) Bin 2, and (c) Bin 3. V_S reductions associated with the negative amplitude peaks A and B and the discontinuities in the velocity models are indicated as % reduction relative to PREM. (d) *S*-wave velocity profile for each bin, showing variability in depth and magnitude of both discontinuities A and B.

models shown. Allowing for trade-offs with density structure increases the uncertainty in both parameters by a corresponding amount. The Fresnel zone for the 0.3 Hz signals is about 400 km long, elongated along the raypath, which averages across our bin dimensions, so the 1D models should not be interpreted as strictly corresponding to the bin regions.

4. Discussion and Conclusion

[14] Our modeling resolves two negative V_S discontinuities within the D″ region under the central Pacific, but no corresponding structure under the Cocos plate. The magnitude of the V_S decreases at each discontinuity under the Pacific are correlated; the weakest discontinuities are in Bin 1, and the strongest discontinuities are in Bin 2. Our 1D models are characterizations of the rapid variations of the wavefield, and need to be smoothed and extrapolated into a 3D structure, with 3D synthetics being constructed to match the data. That is beyond the scope of this paper. A few efforts have been made to model laterally varying ULVZ structure [e.g., *Wen and Helmberger*, 1998], but the data seldom provide much constraint on the model. We have focused here on demonstrating how careful data analysis can guide the development of such laterally varying models.

[15] The V_S reductions of the ULVZ relative to PREM (−3.3% to −7.4%) are not a factor of three stronger than the V_P reduction (−4%) estimated by analogous modeling of *PcP* precursors for this region [*Russell et al.*, 2001], suggesting that partial melt is not the sole origin of the layer, but we have thicker ULVZ layers than used in the corresponding P-wave model. Considering the lateral variability of ULVZ velocity reductions observed in the shear-wave data, an exploration of V_P variability in the ULVZ thickness and velocity drop on comparable scale is necessary to reliably constrain relative variations in V_S and V_P.

[16] Shear velocity discontinuity B was unexpected. Discontinuity B appears to shallow from southwest to northeast across the study region. A 2-layer ULVZ velocity structure has been proposed in other regions [*Rondenay and Fischer*, 2003], but the B discontinuity is significantly shallower and may involve a separate process from that producing the ULVZ. One possibility is that post-perovskite minerals may transform back to perovskite in the steep thermal gradient of the boundary layer above the CMB. A 1–2% V_S decrease would be expected with this back-transformation, coupled to a shallower 1–2% V_S increase [*Hernlund et al.*, 2005; *Flores and Lay*, 2005].

[17] **Acknowledgments.** Data were provided by the IRIS, BDSN, and TRINET data centers. S. Rost and two anonymous reviewers provided helpful comments. This research was supported by NSF grant EAR0125595 (T.L.) and NSF grant EAR0135119 (E.J.G.).

References

Avants, M., T. Lay, S. A. Russell, and E. J. Garnero (2006), Shear velocity variation within the D″ region beneath the central Pacific, *J. Geophys. Res.*, doi:10.1029/2005JB003270, in press.

Dziewonski, A. M., and D. L. Anderson (1981), Preliminary reference Earth model, *Phys. Earth Planet. Inter.*, *25*, 297–356.

Flores, C., and T. Lay (2005), The trouble with seeing double, *Geophys. Res. Lett.*, *32*, L24305, doi:10.1029/2005GL024366.

Garnero, E. J., J. Revenaugh, Q. Williams, T. Lay, and L. H. Kellogg (1998), Ultralow velocity zone at the core-mantle boundary, in *The Core-Mantle Boundary Region*, *Geodyn. Ser.*, vol. 28, edited by M. Gurnis et al., pp. 319–334, AGU, Washington, D. C.

Hernlund, J. W., C. Thomas, and P. Tackley (2005), A doubling of the post-perovskite phase boundary and structure of the Earth's lowermost mantle, *Nature*, *434*, 882–886.

Reasoner, C., and J. Revenaugh (1999), Short-period *P* wave constraints on D″ reflectivity, *J. Geophys. Res.*, *104*, 955–961.

Rondenay, S., and K. M. Fischer (2003), Constraints on localized core-mantle boundary structure from multi-channel, broadband *SKS* coda analysis, *J. Geophys. Res.*, *108*(B11), 2537, doi:10.1029/2003JB002518.

Rost, S., and J. Revenaugh (2003), Small-scale ultralow-velocity zone structure imaged by *ScP*, *J. Geophys. Res.*, *108*(B1), 2056, doi:10.1029/2001JB001627.

Russell, S. A., T. Lay, and E. J. Garnero (1999), Small-scale lateral shear velocity and anisotropy heterogeneity near the core-mantle boundary beneath the Central Pacific imaged using broadband ScS waves, *J. Geophys. Res.*, *104*, 13,183–13,200.

Russell, S. A., C. Reasoner, T. Lay, and J. Revenaugh (2001), Coexisting shear- and compressional-wave seismic velocity discontinuities beneath the central Pacific, *Geophys. Res. Lett.*, *28*, 2281–2284.

Stutzmann, E., L. Vinnik, A. Ferreira, and S. Singh (2000), Constraint on the S-wave velocity at the base of the mantle, *Geophys. Res. Lett.*, *27*, 1571–1574.

Vidale, J. E., and M. A. H. Hedlin (1998), Evidence for partial melt at the core-mantle boundary north of Tonga from the strong scattering of seismic waves, *Nature*, *391*, 682–685.

Wen, L., and D. V. Helmberger (1998), Ultra-low velocity zones near the core-mantle boundary from broadband PKP precursors, *Science*, *279*, 1701–1703.

Williams, Q., and E. J. Garnero (1996), Seismic evidence for partial melt at the base of Earth's mantle, *Science*, *273*, 1528–1530.

M. Avants and T. Lay, Earth Sciences Department, University of California, Santa Cruz, CA 95064, USA. (thorne@pmc.ucsc.edu)

E. J. Garnero, Department of Geological Sciences, Arizona State University, Tempe, AZ 85287-1404, USA. (garnero@asu.edu)